How to evaluate the mass transfer resistances in dense solid–liquid suspensions

How to evaluate the mass transfer resistances in dense solid-liquid suspensions

Giuseppina Montante[a], Alessandro Paglianti[b,*]

[a]Department of Industrial Chemistry, Università di Bologna, via Terracini 28, 40131 Bologna, Italy.
[b]Department of Civil, Chemical, Environmental and Materials Engineering, Università di Bologna, via Terracini 28, 40131 Bologna, Italy.

Abstract

The dissolution of solids in slurry stirred tanks is affected from the solid concentration distribution to different extend, depending on the agitation conditions. In this work, the relationship between solid-liquid mixing and mass transfer is investigated by estimating the characteristic times of different phenomena: liquid mixing, solid dissolution, diffusion of the dissolved species in the vessel volume. The analysis is based on Electrical Resistance Tomography data collected during the simultaneous operations of dissolution and mixing. For dilute solid-liquid systems, the relative importance of the solid dissolution and the liquid mixing depends on the particle size and the impeller speed, while the diffusion in stagnant zones is often negligible. Instead, the diffusion mechanism has an important effect on mass transfer for dense systems, where strong axial gradients of solid concentration are established and the stirred tank volume can be divided into a lower zone containing a cloud of dense mixture and an almost stagnant clear liquid layer on top. Based on original and literature experimental data, a method for the main mass transfer resistance identification depending on the agitation condition, the solid volume fraction distribution and the soluble particle size is suggested.

Keywords: Solid suspension; ERT, mass transfer, dissolution, mixing time, stirred tank.

*Corresponding author. E-mail address: alessandro.paglianti@unibo.it

1. Introduction

The dissolution of solids is a well-known and widely adopted unit operation typically carried out in stirred tanks, where the goal is to achieve a desired rate of dissolution by agitation (Atiemo-Obeng et al., 2004). The increase of production rates in solid-liquid mass transfer operations with respect to existing processes is an important industrial target (Soian et al., 2017), that can be achieved by the selection of optimized geometrical and operating conditions based on deep knowledge and predictive models of the key parameters affecting the overall process. The solid suspension and distribution, the liquid flow field, the solid dissolution characteristics and their interactions importantly affect the performances of the operation. Each of the above mentioned aspects has been separately and extensively investigated by experimental and modelling methods.

The importance of a deep analysis of mixing and dissolution has been addressed in several research works, dealing with chemical (e.g. Tschentscher et al., 2010; El-Naggar et al., 2014; Carletti et al., 2015) and pharmaceutical processes (e.g. Lee et al., 2008; Hörmann 2011), but the interplay of solid-liquid mixing and solid-liquid mass transfer in dense suspensions has been rarely tackled.

After the work of Kikuchi et al. (1987), who observed the effect of high particle concentration on solid-liquid mass transfer, correlating the results with the energy dissipation, a few later works have specifically addressed interaction between fluid dynamics and mass transfer in dense solid-liquid systems. Recently, Bong et al. (2015) have observed that the dependency of solid-liquid mass transfer from the solid concentration effects exhibits a maximum value that is probably related to the variation of the just suspended impeller speed and the consequent turbulent level around the particles. Stoian et al. (2017) extended the investigation to a dual impeller stirred tank and compared baffled and unbaffled configurations. The importance of considering the suspension state was more recently addressed by Carletti et al. (2018) and Tokura et al. (2019) in dilute solid-liquid systems,

This work is aimed at investigating the interactions of solid suspension, solid distribution, liquid mixing and solid-liquid mass transfer in dilute and dense solid-liquid systems for identifying the limiting step of the dissolution process, depending on the properties of the soluble particle size and on the agitation conditions.

Solid suspension, solid distribution, liquid mixing have been separately and extensively investigated so far, as recently reviewed by Mishra and Ein-Mozaffari (2020), while comparatively a much smaller amount of work has been carried out on solid dissolution especially in dense suspensions. The complex dependency of the liquid mixing time on the solid concentration and on the clear liquid layer height in dense systems has been already highlighted in previous works (Kraume et al.,

1992; Bujalski et al., 1999) leading to interesting conclusions, which impact on solid dissolution has never been considered. The presence of a clear liquid layer above a dense solid suspension region has important effects on the liquid mixing time, but also on the micromixing and therefore on the selectivity of competitive chemical reactions (Hofinger et al., 2011).

As a difference with previous investigations, in this work the diffusion of the dissolved species in the clear liquid layer that usually establishes in dense solid-liquid systems is specifically considered. The experiments are performed by the Electrical Resistance Tomography (ERT) technique, that provides local conductivity data on several locations of the vessel without being intrusive.

The paper is organized as follows: in the next section, the stirred tanks, the solid-liquid systems and the Electrical Resistance Tomography technique adopted for collecting the experimental data are presented. Afterwards, the correlations for estimating the characteristic times for solid dissolution, liquid homogenization and species diffusion in the stagnant vessel zone are presented and the methodology for their adoption for establishing the main mass transfer resistance in dilute and dense solid-liquid systems is described. Then, based in original and previous data, a method for estimating the location of the interface between the clear liquid layer and the solid suspension for a wider range of experimental conditions with respect to existing correlations is presented. The ERT data are adopted for estimating the solid-liquid mass transfer rate by the comparison of the above mentioned characteristic times in dilute and dense systems, taking into account the possible presence of a clear liquid layer and its height. Finally, a method for estimating the prevailing mass transfer resistance depending on the particle size and the agitation conditions is suggested.

2. Material and methods

2.1 The stirred tank configurations and the investigated solid-liquid systems

The investigation was carried out in cylindrical, flat bottomed stirred vessels made of Plexiglas of diameter, T, equal to 0.232 m (T23) and 0.480 m (T48), respectively, equipped with four equally-spaced baffles of width equal to T/10. Agitation was provided with different impeller types: a single 4-bladed 45° down-pumping pitched blade turbine (PBT), a Rushton turbine (RT) and a Lightnin A310 impeller (A310) mounted on a central shaft, located at the off-bottom clearance, C, of T/3. PBT and A310 impellers were used in T23 and their diameter, D, was equal to 0.096 m and 0.078, respectively. Rushton turbines were used in T23 and T48 and the diameter was 0.078 m and 0.15 m, respectively.

The experiments were performed injecting a saturate aqueous solution of NaCl or adding NaCl in grains in the vessel at different impeller speeds, N. For the solid dissolution experiments, a narrow

size distribution of the grains was obtained by sieving (mean diameter, d_p, equal to 0.375, 1.59 and 3 mm, ρ_s=2163 kg/m^3). The particle mean size adopted in the following, d_p, is the arithmetic mean of the upper and the lower sieve size, as suggested by Nienow (1969). The vessel volume was preliminary filled with water or with a dense suspension of inert solid particles in water. In the latter case, the inert solid phase consisted of sieved glass particles (mean diameter, d_i, equal to 133 and 385 μm, mass ratio of inert solid to liquid, X, 0.29 and 0.43, density, ρ_i=2500 kg/m^3). In all cases, a small amount (0.5 g/L) of sodium chloride was added in the demineralized water to obtain an appropriate and reproducible electrical conductivity.

The total liquid height, H_L, was maintained at 0.23 m, corresponding to a total volume of 9.6 L for T23 and 0.48 m for T48, corresponding to a total volume of 86.9 L. The experiments were carried out at room temperature of 20°C±2°C in batch conditions.

2.2 The Electrical Resistance Tomography technique

The liquid mixing and the solid dissolution dynamics were measured by the ITS P2000 Electrical Resistance Tomography (ERT) instrumentation (Industrial Tomography Systems Ltd.), by which the distribution of the electrical conductivity was measured as a function of time on four horizontal vessel sections. The vessel periphery was provided with 16 equally spaced electrodes, made of squared stainless steel plates fixed to the internal vessel wall, as shown in Figure 1. The geometrical details on the electrodes and the position of the measurement planes are shown in Table 1. The impeller was located between the planes z_1 and z_2. The electrodes were connected to the data acquisition system by coaxial cables for reducing the effect of noise and interference.

	T23	**T48**
Tank diameter, T [m]	0.23	0.48
Elevation of the measurement planes, z [m]	0.06, 0.11, 0.16, 0.21	0.18, 0.30, 0.42, 0.54
Square electrode side [m]	0.020	0.032
Electrode thickness [m]	0.001	0.002
Number of electrodes per plane	16	16

Table 1 Geometrical characteristics of the electrodes set-up for ERT measurements.

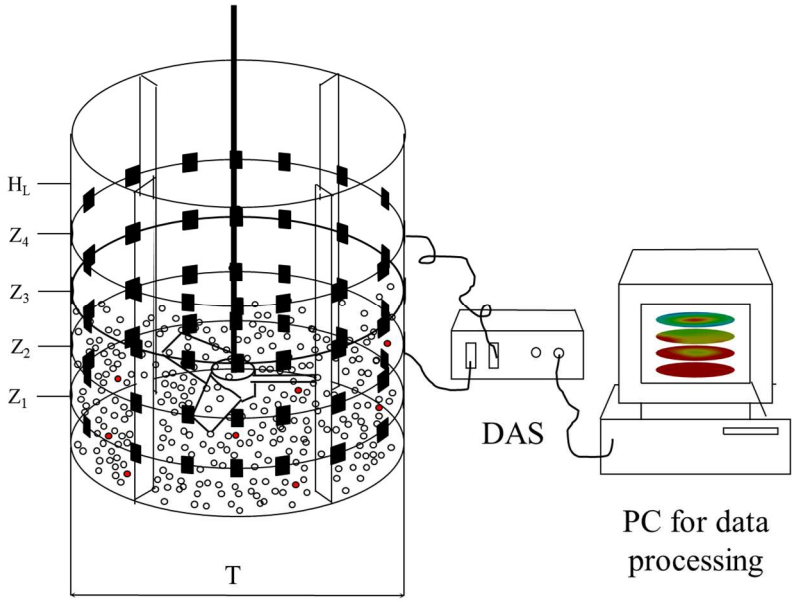

Figure 1. ERT experimental set up.

The measurement is based on the injection of a current between a pair of electrodes and the determination of the resultant voltage difference between the remaining electrodes. The procedure is repeated for all pairs of electrodes, thus allowing to collect 104 voltage values. Details on the technique working principles can be found elsewhere (Stanley et al., 2002, Montante et al., 2015).

The amplitude of 15 mA and the injected current frequency of 9600 Hz were adopted, similarly to previous investigations (Paglianti et al., 2020, Carletti et al., 2018). The number of recorded frames was varied from 1500 to 3000 depending on the total time required for the complete homogenization. In all cases, the acquisition was started 20 s before the dissolved or solid salt addition. The time resolution of the collected time trace was equal to 0.24 s, resulting from the acquisition of 4.2 frames per second. The local conductivity was obtained on a square grid of side equal to 11.5 mm in T23 and to 24 mm in T48. The number of cells per plane was equal to 316 in both cases. As for the reconstruction method for obtaining the conductivity maps from the voltage difference, the linearized (non-iterative) back projection algorithm was selected (Williams & Beck, 1995), as implemented in the ITS System p2+ V8 software. The reconstruction of the conductivity maps was very fast, thus the conductivity distribution was monitored in real time. The number of local measurements inside each circular tomogram, n, was equal to 316, thus, when considering the 4 investigated planes, a total number of conductivity values equal to 1264 was obtained.

The measured dimensionless conductivity in the cell i, $C_i(t)$, is adopted for the estimation of the local tracer homogenization dynamics after a suitable normalization, being it proportional to the tracer concentration. The normalized local conductivity, χ_i, is calculated as:

$$\chi_i(t) = \frac{C_i(t) - C_i(0)}{C_i(\infty) - C_i(0)} \quad (1)$$

where $C_i(0)$ and $C_i(\infty)$ are the initial (before the tracer addition) and the final (after the complete homogenization) conductivity in the cell i, respectively. In the following the mean value of the normalized conductivity on the n local measurement on each plane ,$\bar{\chi}$, is also used.

3. Theory and calculations

3.1 The evaluation of the characteristic times

In stirred tank treating solid-liquid mixtures, different types of mass transfer resistances can be encountered, depending on the particular system and working conditions. In this work, the following physical phenomena and relevant characteristic times will be considered: a) the solid dissolution, usually evaluated by means of the mass transfer coefficient and the particle size; b) the liquid homogenization, usually evaluated by means of the mixing time; c) the homogenization of dissolved species in stagnant zones in the vessel, if any, whose characteristic time is evaluated by means of the penetration theory (Treybal, 1981).

3.1.1 Evaluation of the characteristic time required for the solid dissolution

The characteristic time of the dissolution process can be evaluated from the integration of the mass balance on a single grain. As originally proposed by Nienow and Miles (1978), the following correlation can to be used for estimating the time required to achieve the complete dissolution of particles of size d_p:

$$t_d = \frac{\rho_s d_p^2}{Sh\, D_j\, 2\, (C_{sat} - C_{bulk})} \quad (2)$$

where C_{sat} and C_{bulk} are the salt concentration in the saturated conditions and in the liquid bulk respectively, D_j is the diffusion coefficient of dissolving species and *Sh* is the Sherwood number estimated by the correlation recently suggested by Carletti et al. (2018), as:

$$Sh = 2 + 0.0096 \left(\frac{D}{C}\right)^{2/3} Re_p^{2/3}\, Ar^{0.16}\, Sc^{1/3} \quad (3)$$

where Re_p, Ar and Sc are the particle Reynolds number, the Archimedes number and the Schmidt number, respectively.

3.1.2 Evaluation of the characteristic time required for the liquid homogenization

The liquid homogenization after the instantaneous addition of a tracer to a batch stirred tank has been widely analyzed in the last two decades and consensus on the very well-known equation suggested by Grenville is achieved for the mixing time estimation in single-phase, single impeller, fully turbulent stirred tanks (Grenville and Nienow, 2004). In this work, the modified form suggested by Magelli et al. (2013) will be considered, since it is extends the correlation of Grenville to tanks with multiple impellers and height to diameter ratio, H_L/T, different from 1. The correlation reads as:

$$t_{m,95} = 2.4 \left(\frac{\pi}{4}\right)^{\frac{1}{3}} \frac{1}{N_Q N} \left(\frac{T}{D}\right)^2 \frac{H_L}{D} \tag{4}$$

where $t_{m,95}$ is the time required to achieve the 95% of the liquid homogeneity, N_Q is the impeller flow number, (Magelli et al., 2013).

To compare this value with the t_d, a strict criterion for the liquid homogenization is required, therefore in the following the mixing time is referred to the 99.9% instead of the 95% homogeneity level. Assuming that the process occurs as a first order process, the following correlation is usually adopted:

$$t_{m,x} = t_{m,95} \frac{\ln\left(1-\frac{x}{100}\right)}{\ln(1-0.95)} \tag{5}$$

Therefore, under the hypothesis that the complete homogenization occurs at x=99.9%, the following mixing time correlation is obtained:

$$t_m = 7.37 \left(\frac{\pi}{4}\right)^{\frac{1}{3}} \frac{1}{N_Q N} \left(\frac{T}{D}\right)^2 \frac{H_L}{D} \tag{6}$$

3.1.3 Evaluation of the characteristic time for the homogenization of stagnant zone

The analysis of the solid-liquid fluid dynamics of stirred tanks working with high amount of solids showed that, depending on the impeller speed, an almost stagnant clear liquid layer can be present in the upper part of the tank (Bujalski et al., 1999). In this case, the characteristic time required for the liquid homogenization cannot be described with the same equations adopted for single-phase or dilute solid-liquid stirred vessels (Sardehpande et al., 2009). To account for the sharp difference between the two regions of the vessel delimited by the interface between the suspension and the clear liquid layer, the following simplified approach is proposed.

According to the penetration theory (Treybal, 1981), the mass transfer coefficient at the interface between the clear liquid layer and the suspension can be evaluated as:

$$k_{diff} = 2\sqrt{\frac{D_j}{\pi\, t_r}} \tag{7}$$

Where D_j is the molecular diffusivity and t_r is the typical "contact time" of the eddies at the interface during one cycle. Assuming that, $1/t_r$, that is the frequency of the eddies, is proportional to the impeller speed, N, the mass transfer coefficient can be estimated as:

$$k_{diff} \propto 2\sqrt{\frac{D_j\, N}{\pi}} \tag{8}$$

Based on Eq. (8), the characteristic time for the homogenization of the stagnant zone is evaluate as:

$$t_{diff} \propto \frac{H_L - H_C}{2\sqrt{\frac{D_j N}{\pi}}} \tag{9}$$

Where H_L is the liquid height and H_C is the cloud height.

It is important to note that the estimation of the mass transfer coefficient in slurry stirred tanks might be further improved, taking into account that the clear liquid layer is very quiescent (Hofinger et al., 2011), but not perfectly stagnant.

3.2 Identification of the main mass transfer resistance

Mass transfer resistances in solid-liquid stirred tanks may strongly change with the location, depending on the physical properties of the phases and on the operating conditions. To take into account the significant difference between dense and dilute solid-liquid systems, the analysis of dense systems, where a cloud of dense suspension can be present and that of dilute conditions, where the cloud cannot be formed, are treated separately. Indeed in the latter case, absence of stagnant zones makes the description of the mass transfer mechanisms definitely closer to the case of single-phase systems, while in the former, a specific description is required.

3.2.1 Dilute solid-liquid systems

In dilute solid-liquid systems, the solids can be either inert or soluble particles. In the former case, the variation of the liquid concentration due to the addition of a different miscible liquid phase practically occurs with the same mechanisms and characteristic times of single-phase stirred tanks. Instead, in the case of soluble particles, two interacting phenomena occur: the particles dissolution and the mixing of the liquid phase. To estimate which of the two processes will be the mechanism controlling the mass transfer dynamics in the stirred tank, the ratio between t_m and t_d is considered.

For stirred tanks with aspect ratio equal to 1 and under the simplified hypothesis that $C_{bulk} \approx 0$, that is reasonable for small soluble particle concentrations, the ratio between Eqs. (2) and (6) is:

$$\frac{t_d}{t_m} = \frac{\left(\frac{4}{\pi}\right)^{1/3}}{14.74} \frac{N_Q\, N\, \rho_s d_p}{k_L\, C_{sat}} \left(\frac{D}{T}\right)^3 \tag{10}$$

If $t_d >> t_m$ the characteristic time of the process will be mainly determined by the particle dissolution, while if $t_m >> t_d$ the mixing process will control the dissolution.

3.2.2 Dense solid-liquid systems

The liquid mixing time

Liquid mixing time in dense solid-liquid systems is clearly affected by the presence of the clear liquid layer. When a miscible liquid mixture is added to the tank, the liquid homogenization is characterized by the presence of two resistances: the former due to the liquid mixing promoted by the impeller action, whose characteristic time is t_m, and the latter due to the presence of the clear liquid layer, whose characteristic time is t_{diff}. The simplest way to compare the two phenomena is by the ratio between the two characteristic times t_m/t_{diff} that is:

$$\frac{t_m}{t_{diff}} = \frac{14.74}{4^{1/3}\pi^{1/6}} \frac{1}{N_Q} \frac{H_L}{H_L - H_C} \left(\frac{T}{D}\right)^2 \frac{\sqrt{\frac{D_j}{N}}}{D} \tag{11}$$

where t_m is evaluated as in single phase and dilute systems.

The soluble solid dissolution

The mass transfer from soluble particles to a dense suspension of inert solids can be affected by three different resistances: a) the resistance due to the particle dissolution, b) the resistance due to the liquid mixing and c) the resistance due to the presence of a stagnant liquid layer. In Figure 2, a schematic qualitative diagram showing the range of existence of the three resistances is shown.

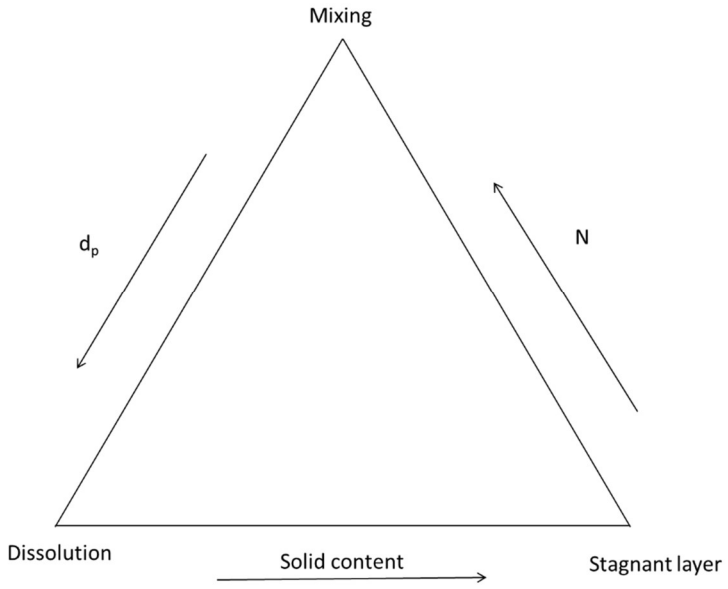

Figure 2. Schematic diagram with the different resistances.

For tiny soluble particles, the resistance due to the dissolution process is expected to be negligible and therefore the two resistances that have to be compared are due to the stagnant liquid zone and to the liquid mixing, similarly to the case of the homogenization of a miscible liquid phase. For very high impeller speed, ensuring the solid phase distribution up to the vessel top and the disappearance of the stagnant clear liquid zone, the two resistances that have to be analyzed are due to the solid dissolution and the liquid mixing. In the process industry, the solid dissolution process is often carried out using relatively coarse soluble grains and modest impeller speeds, for limiting the energy consumption of the milling processes and of the mechanical agitation. Therefore, under the conditions that are most likely adopted in the industrial operations, the two dominant resistances are due to the dissolution and to the presence of a stagnant liquid layer. The ratio of the relevant times is:

$$\frac{t_d}{t_{diff}} = \frac{\rho_s d_p^2}{Sh\, D_j\, (C_{sat} - C_{bulk})} \frac{\sqrt{\frac{D_j N}{\pi}}}{H_L - H_C} \tag{12}$$

If the dissolved species concentration in the bulk is negligible with respect to the saturation concentration of the soluble particles and the Sherwood number is defined as $\frac{k_L d_p}{D_j}$, Eq. (12) becomes:

$$\frac{t_d}{t_{diff}} = \frac{\rho_s d_p}{k_L\, C_{sat}} \frac{\sqrt{\frac{D_j N}{\pi}}}{H_L - H_C} \tag{13}$$

4. Results and discussion

4.1 Location of the interface between the cloud height and the clear liquid layer in dense systems

A prerequisite for a realistic estimation of the mass transfer resistances in the dissolution of solids in dense suspensions of settling solids is the capability to determine possible stagnant zones in the upper part of the vessel due to presence of a clear liquid layer and, in case of existence, the elevation of the interface between the suspension and clear liquid layer, H_C.

Following Bittorf and Kresta (2003), H_C can be obtained from the following equation, strictly valid for A310 and HE3 impellers with D/T less than or equal to 0.52.

$$H_C = H_L \frac{N}{N_{js}} \left[0.84 - 1.05 \frac{C}{H_L} + 0.7 \frac{\left(\frac{D}{H_L}\right)^2}{1-\left(\frac{D}{H_L}\right)^2} \right] \tag{14}$$

At equal geometrical characteristics of the tank and physical properties of the solid-liquid system, Eq. (14) shows that the cloud height linearly increases with the impeller speed. Additional experimental investigations performed by Bujalski et al. (1999) and Brunazzi et al. (2004) have shown that at low impeller speeds due to the limited quantity of the suspended particles, the solids are suspended up to the liquid top surface. In the following, a possible extension of the correlation by Bittorf and Kresta (2003) is explored, to predict H_C also for incomplete suspension conditions ($N< N_{JS}$). The just suspended impeller speed, N_{JS}, fixes the boundary between stirred tanks working with the solid phase fully suspended and those working with part of the solid phase settled on the tank bottom. Therefore, to extend the application of the Bittorf and Kresta correlation in the range of the low impeller speeds, the influence of amount of the settled solid phase has to be considered. The suspended solid fraction, that is the ratio between the mass of suspended solid and the total mass of solid in the stirred tank can be predicted by the simplified correlation of Micale et al (2002), as:

$$X_s = 1 - exp\left[-\left(\frac{N - N_{min}}{N_{span}} \right)^2 \right] \quad \text{for } N \geq N_{min} \tag{15}$$

Where N_{min} is the agitation speed at which the suspension phenomenon starts and N_{span} is a parameter that is a function of the particles diameter and of the solid concentration. In this work N_{min} and N_{span} have been evaluated as suggested by Micale et al. (2002).

The correlation is useful for estimating the fraction of settled solids with respect to the total mass of solids and liquid in the vessel and the possible relationship with the cloud height achieved from the suspension. Being (1-X_s) the fraction of the non-suspended solid, X the solid mass ratio, that is the mass of solid divided by the mass of liquid in the vessel and X/(1+X) the solid mass fraction, the ratio between mass fraction of the settled solid with respect to the total solid-liquid mixture in the stirred tank, X_{US}, can be estimated as: $\frac{(1-X_S)\,X}{(1+X)}$.

The cloud height measured from Bujalski et al. (1999) is reported in Figure 3 as a function of X_{US}.

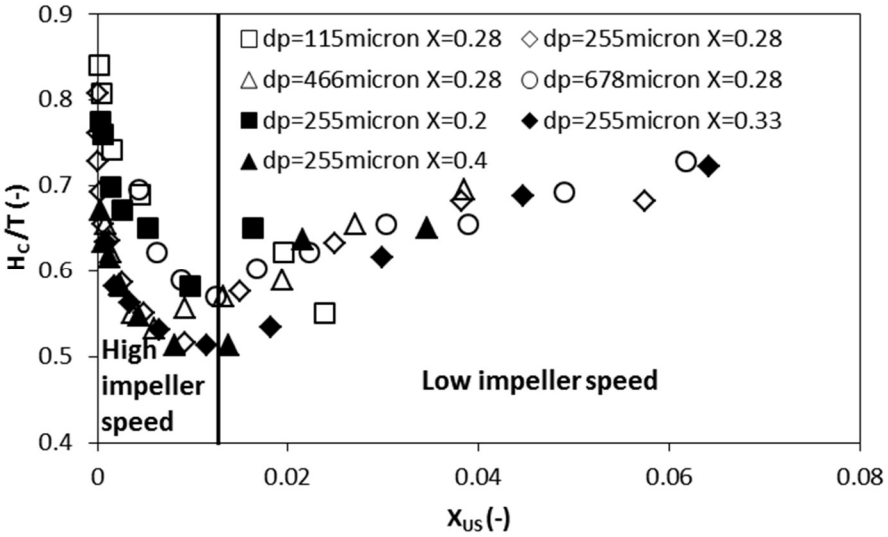

Figure 3. Effect of the suspended fraction on the cloud height. Experimental data from Bujalski et al. (1999).

The experimental data show that the cloud height has a minimum value equal to 0.5T approximately at $X_{US} = 0.014$. Based on Figure 3, the behavior of the solid suspension can be divided in two zones. Experimental data with $X_{US} < 0.014$ are relevant to high impeller speeds, where the Bittorf and Kresta correlation can be used, while for $X_{US} > 0.014$ the data have been obtained at low impeller speed, where the Bittorf and Kresta correlation largely underpredicts the cloud height. The data scatter observable for $X_{US} < 0.014$ evidences that H_C/T does not depends only from the amount of the suspended solid but, as suggested by Bittorf and Kresta, it is also a function of N_{js}.

In this work, for stirred tank with H_L=T if $X_{US} < 0.014$ the equation suggested by Bittorf and Kresta has been used, while for $X_{US} > 0.014$ the following equation is suggested,:

$$H_C = H_L \frac{X_{US}+0.029}{X_{US}+0.065} \tag{16}$$

A comparison between experimental data and the modified equation by Bittorf and Kresta is shown in Figure 4.

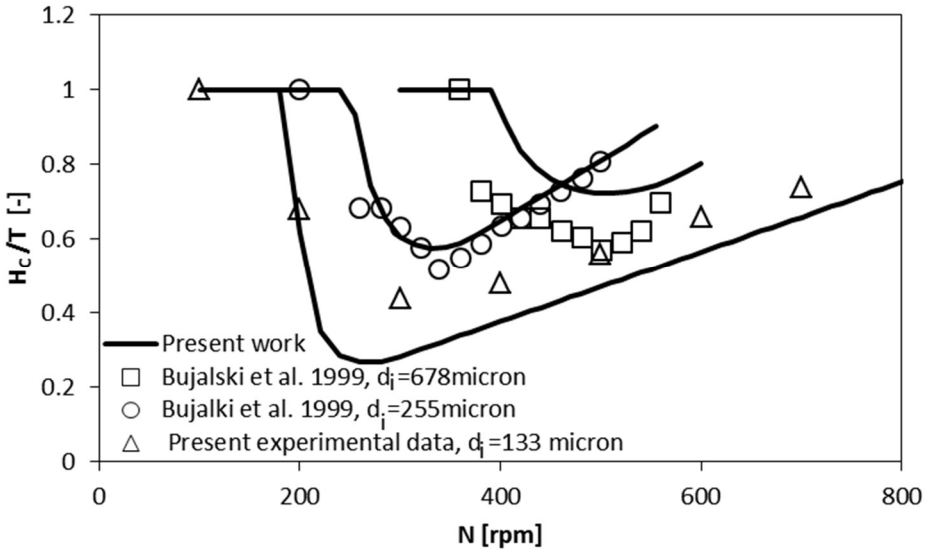

Figure 4. Comparison between present correlation and experimental data, A310 impeller. Present data: d_I 133μm, X=0.29, T23. Bujalski et al. (1999) data: d_i 255 and 678 μm, X=0.28, T29.

The possibility to estimate the elevation achieved by the solid particles in a wide range of impeller speeds is a necessary preliminary step in the case of dense solid-liquid stirred tanks, for evaluating a) the effect of the clear liquid layer on the liquid mixing; b) the effect of the clear liquid layer on the dissolution process.

4.2 Analysis of solid-liquid mass transfer

The liquid mixing, the soluble solid dissolution and the inert solid distribution in stirred tanks can be all effectively investigated by the ERT technique. The typical experimental outcome of the measurements is the time dependent evolution of the mean normalized dimensionless conductivity on a plane $\bar{\chi}$, as that shown in Figure 5, or tomograms showing the local values of the same parameter χ_i, as those reported in Figure 6. Qualitative or quantitative information can be obtained from the data analysis. For instance, the mean dimensionless concentration on the z_4 plane reported in Figure 5 shows that the time to reach the steady state value is longer in the upper plane probably due to the stagnant clear liquid layer, that forms under the selected operating conditions, as shown in Figure 4. The analysis of the time traces allows to evaluate the $t_{m,95}$, that in this specific case is equal to 57 s.

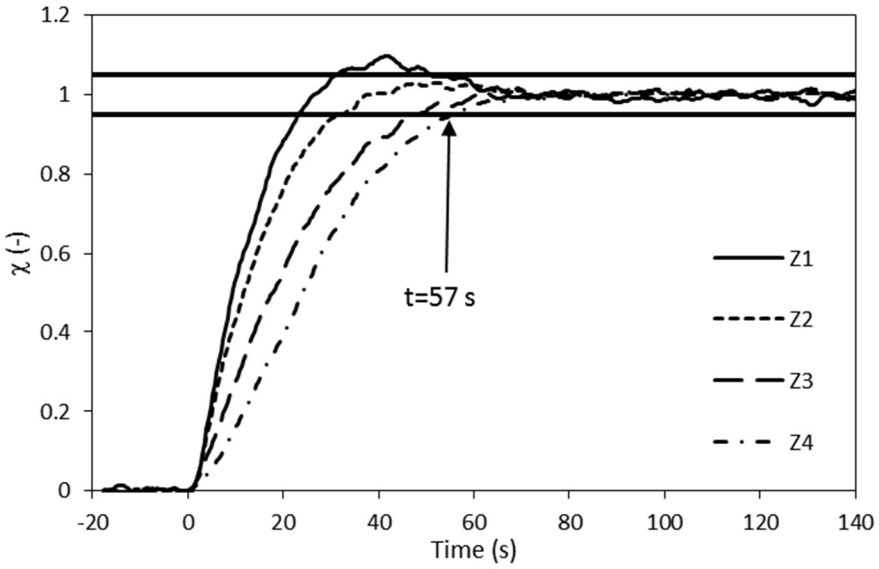

Figure 5. Example of the time trace of the mean conductivities on the four measuring planes. T23 A310, N = 600 rpm, d_i=133μm, X=0.29, d_p=1.6 mm.

Figure 6 shows the typical local information that can be obtained by ERT. The presence of the clear liquid layer clearly affects the liquid homogenization. In the working conditions adopted in the experiments showed in Figure 6, during the first 15 seconds after the tracer addition, the local conductivity in most of the locations in the upper measuring plane remains low, while in the lower planes it approaches the steady state value much faster. This means that the liquid mixing dynamics strictly depends on the inert solid distribution in the vessel volume and the ERT data can provide quantitative information on these aspects.

Based on the ERT investigation of the stirred tanks described in Section 2, the methodology for the identification of the prevailing mass transfer resistances in dilute and dense suspension of solids will be applied to the analysis of original data and previous results available in the literature.

The analysis will be organized as follows.

- Dilute solid-liquid system: in this case the analysis will be limited to the dissolution of a soluble solid in water, based on the experimental data collected by Carletti et al. (2018). The liquid mixing in single-phase and very dilute solid-liquid systems has been extensively examined in the past decades.
- Dense solid-liquid systems: the homogenization of a miscible liquid, based on original data collected in this work and the literature data by Bujalski et al., (1999), Carletti et al. (2016), Paglianti et al. (2017).

- Dense solid-liquid systems: the dissolution of a soluble solid, based on original data collected in this work.

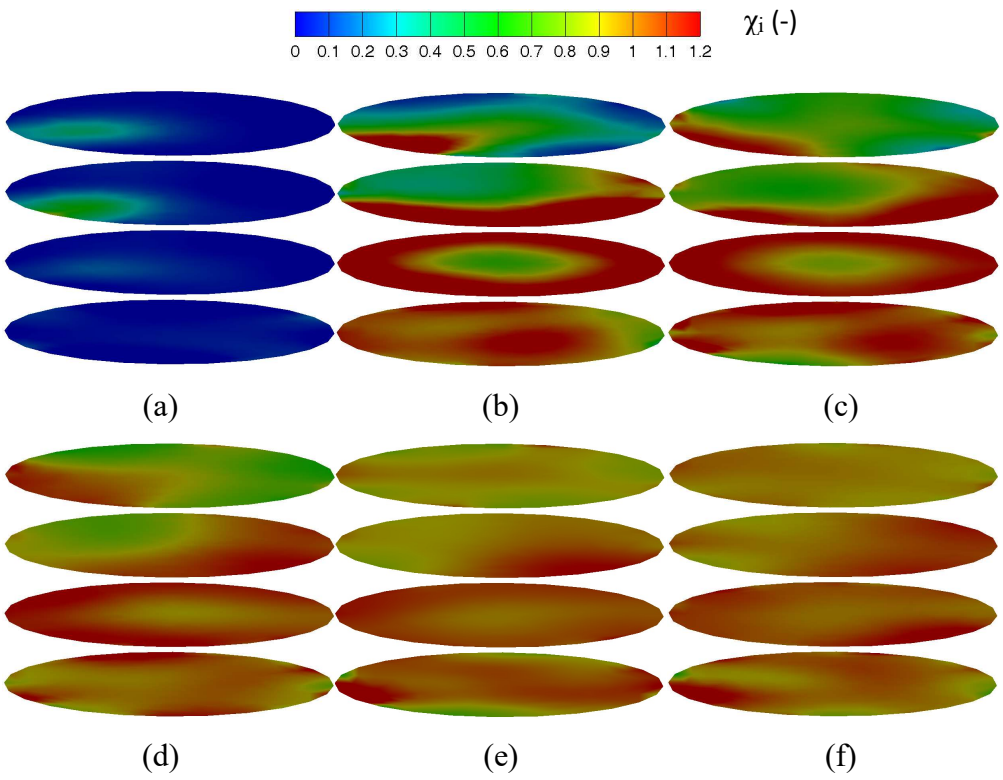

Figure 6. Example of the normalized conductivity maps (χ_i) at selected times during the liquid homogenization. T23 A310, N = 500 rpm, d_i=385µm, X=0.43. (a) t = 1 s; (b) t = 5 s; (c)t = 10 s; (d) t = 15 s; (e) t=20; (f) t=25.

4.2.1 Analysis of dilute systems

The analysis is based on the data collected during the dissolution of NaCl grains in vessels of two sizes (T23 and T48) stirred with a RT in a conventional arrangement (D=T/3; C=T/3). The ratio between the dissolution time estimated from the experimental data and from Eq. (2) is observed as a function of the ratio between the dissolution time and the mixing time estimated by Eq. (10) in Figure 7. The experimental dissolution time, $\tau_{dis,dil}$, is estimated from the experimental mean dimensionless conductivity curves as the time required to reach the 95% of the final value. The estimation of the 99.9% dissolution time was renounced, due to the signal fluctuations, which do not allow a precise estimation.

Figure 7 shows that for $\frac{t_d}{t_m}$ >2, $\frac{\tau_{dis,dil}}{t_d}$ varies slightly, showing a weak dependency on the tank diameter, working conditions and grain size. While for $\frac{t_d}{t_m}$< 2, the value of $\frac{\tau_{dis,dil}}{t_d}$ is higher and the variation is more marked. Since $\frac{t_d}{t_m}$ gives the ratio between the characteristic times of dissolution and mixing, large values of this ratio correspond to working conditions at which the main mass transfer resistance is due to the dissolution of the particles. Vice versa, when the particles size is below a critical value the characteristic time for the dissolution becomes less important than the characteristic time due to the liquid mixing, as in present case when the grains size is equal or below 1.24 mm. Figure 7 shows that the main resistance can be identified by using Eq. 10. For the systems investigated in this work, the threshold value of the computed time ratio equal to 2 identifies a transition from the liquid mixing to the dissolution controlled regimes.

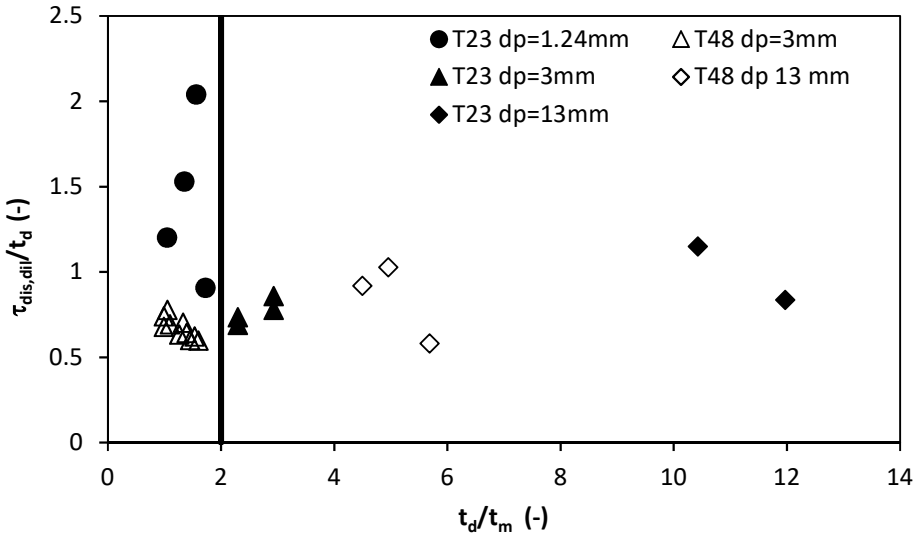

Figure 7 Experimental data on dissolution process in dilute conditions.

4.2.2 Liquid mixing time in dense solid-liquid suspensions

The liquid mixing time in dense suspensions of inert solids obtained with the PBT and the A310 impellers in the T23 are considered in the following. The computed data obtained using Eq.14 have been compared with the experimental data plotted in the dimensionless form, as the ratio between the experimental 95% mixing time, $\tau_{mix,dense}$, divided by the computed t_m by Eq. 4, in Figure 8. Although large differences between the results obtained with two impellers are apparent, the

experimental value of $\frac{\tau_{mix,dense}}{t_m}$ increases to values largely greater than one, if the ratio $\frac{t_m}{t_{diff}}$ is lower than 0.02-0.03.

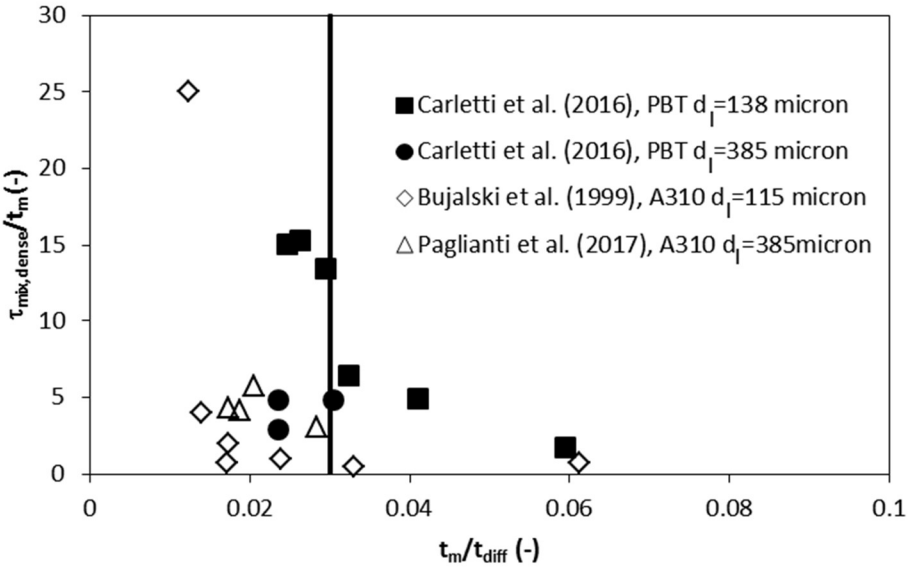

Figure 8. Experimental data on homogenization process in dense suspensions. Bujalski et al. (1999): X=0.2; Paglianti et al. (2017): X=0.43; Carletti et al. (2016): X=0.43.

Because t_{diff} is large when a clear liquid layer takes place, small values of $\frac{t_m}{t_{diff}}$ are associated to working condition with the presence of a clear liquid layer.

The experimental data shown in Figure 8 clearly suggest that if the ratio $\frac{t_m}{t_{diff}}$ is greater than the critical value 0.02-0.03 the experimental values of the ratio $\frac{\tau_{mix,dense}}{t_m}$ are close 1, this means that the mixing time can be roughly evaluated as in single phase flow, using Eq. 6. Instead, if $\frac{t_m}{t_{diff}}$ is smaller than 0.02-0.03, a clear liquid layer appears on the top of the tank and the use of Eq. 6 can induce a large underestimation of the time necessary to achieve the homogenization of the equipment.

4.2.3 Solid dissolution in dense solid-liquid suspensions

The dissolution of soluble particles in dense suspension of inert solids was observed adopting the PBT and the A310, since they are suitable for the solid suspension in stirred tanks. The inert solids were glass ballotini of different size and mass ratio (d_i= 385 μm and X=0.43 with the PBT; d_i=133 μm and X=0.23 with the A310). In both cases soluble NaCl grains of three different mean sizes

(d_p=0.375, 1.59 and 3 mm) were added to the solid-liquid suspension and their dissolution was monitored by ERT at variable impeller speeds, covering a wide range of conditions, including suspensions with a clear liquid layer on the vessel top.

As in the case of the dissolution in dilute systems, the experimental liquid mixing time was estimated considering the achievement of the 95% of the liquid conductivity value after the complete solid dissolution. The experimental mixing time was made dimensionless by the value computed by Eq. 2.

As a difference with the previous systems, in this case three different mass transfer resistances can occur, that are associated to solid dissolution, liquid mixing or molecular diffusion in an almost still liquid. The evolution of the normalized conductivity when large or small soluble particles are added to a dense solid-liquid mixture are shown in Figures 9 for particles of the larger (3 mm) and the smaller (0.375 mm) size.

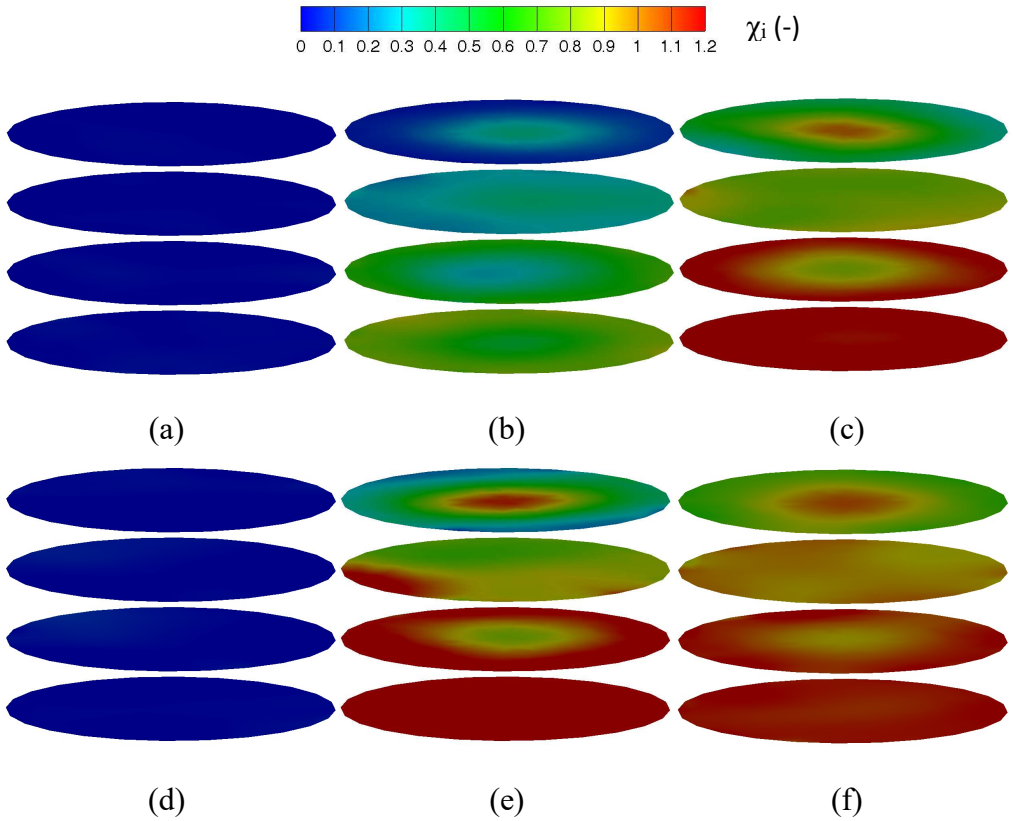

Figure 9. Example of the normalized conductivity maps (χ_i) at selected times during the salt dissolution. T23 A310, N = 400 rpm, X=0.23, NaCl. (a) d_p = 3 mm, t = 1 s; (b) d_p = 3 mm, t = 22 s; (c) d_p = 3 mm, t = 88 s; (d) d_p = 0.375 mm, t = 1 s; (e) d_p = 0.375 mm, t = 22 s; (f) d_p = 0.375 mm,t=88 s.

Observing the lower sections in the Figures 9 (b) and 9 (e), it is possible to notice that in the lower part of the tank the value of the normalized conductivity increases quicker for the smaller particles, because of the faster dissolution. Moreover, for both the soluble particle sizes, the experimental data highlight that the normalized conductivity is higher close to the bottom than in the upper part of the tank. This behavior can be associated to the presence of the dense solid-liquid suspension up to z/T=0.4 and to the clear liquid layer for higher elevations. Clearly, in the almost stagnant clear liquid zone an additive diffusive mass transfer resistance slows down the homogenization of the dissolved salt in the liquid.

In Figure 10 the ratio $\frac{\tau_{dis,dense}}{t_d}$ is plotted against the ratio $\frac{t_m}{t_{diff}}$ computed by Eq. 11., the critical value is 0.03, that is the same identified in Figure 8.

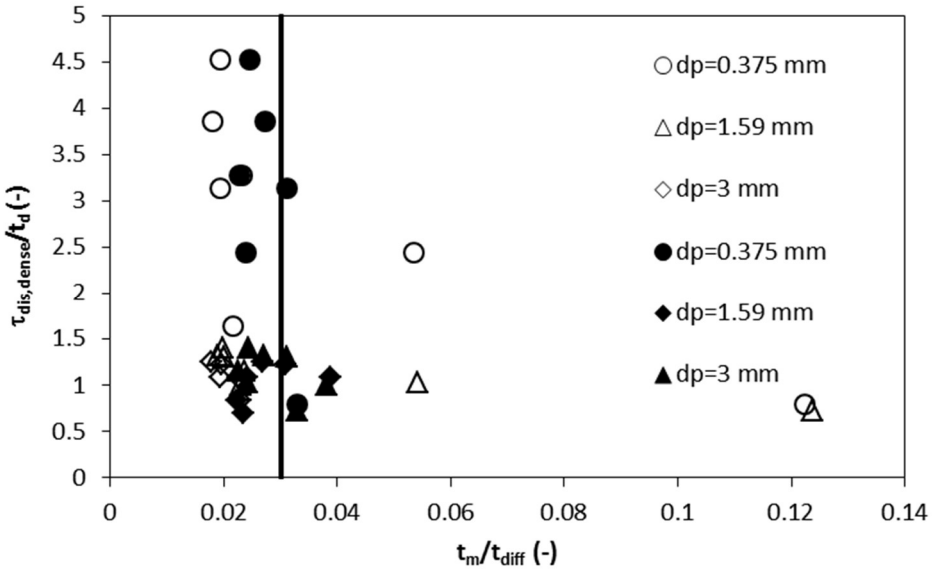

Figure 10. Experimental data on dissolution process in dense conditions, comparison between mixing and diffusion resistances. Open symbols A310 d_I 133μm, X=0.29, T23, solid symbols PBT d_I=385μm, X=0.43, T23.

As can be observed, for the smaller particles the experimental dissolution time is greater than the t_d value evaluated with Eq. 2, suggesting that the main resistance to the homogenization process is not the dissolution of the particles, but the homogenization of the liquid phase. For larger particles, the ratio $\frac{\tau_{dis,dense}}{t_d}$ is close to 1, indicating that the main resistance of the homogenization process is the

particle dissolution. The threshold that allows to discriminate between the two conditions can be assumed as $\frac{t_m}{t_{diff}}$ equal to 0.03.

Considering the ratio $\frac{t_d}{t_{diff}}$ evaluated by Eq. 13 and shown in Figure 11, for values greater than 0.03 the ratio $\frac{\tau_{dis,dense}}{t_d}$ assumes practically a constant value. If the stirred tank works in these conditions, the characteristic time for the homogenization can be evaluated as the time necessary to dissolve the soluble particles, even if the system is a dense system. While if $\frac{t_d}{t_{diff}}$ is smaller than 0.03, that occurs when the characteristic size of the dissolving particles is below a critical value, the main resistance is not anymore the dissolution of the soluble particles, but it becomes the mixing/diffusion process in the tank.

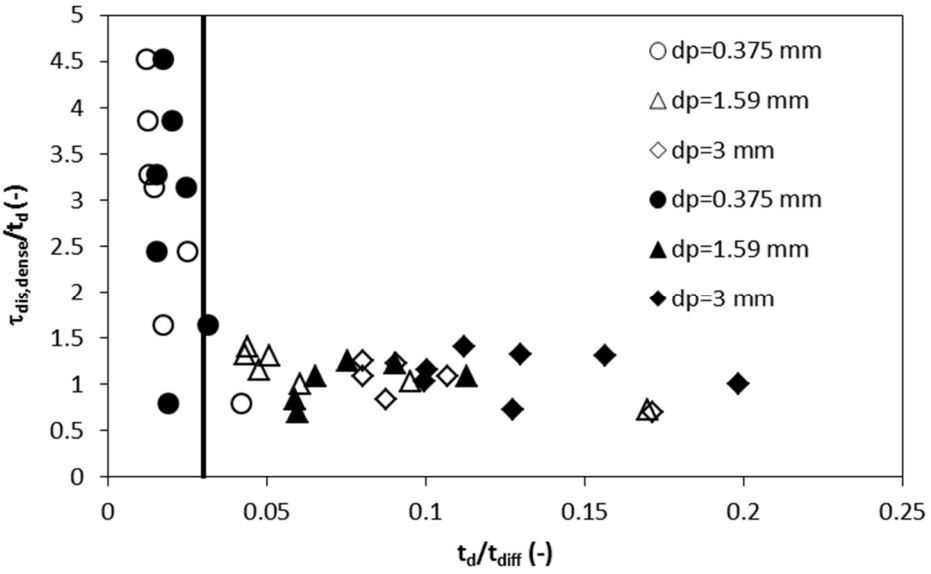

Figure 11. Experimental data on dissolution process in dense conditions, comparison between dissolution and diffusion characteristic times. Open symbols A310 d_I 133µm, X=0.29, T23, solid symbols PBT d_I=385µm, X=0.43, T23.

Figure 12 shows the same data plotted against the ratio $\frac{t_d}{t_m}$

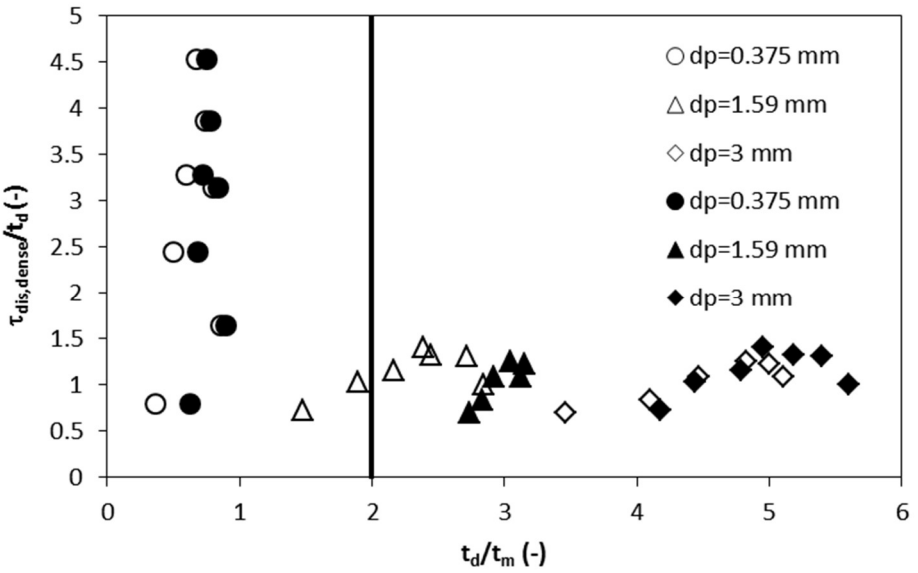

Figure 12. Experimental data on dissolution process in dense conditions, comparison between dissolution and mixing characteristic times Open symbols A310 d_I 133μm, X=0.29, T23, Solid symbols PBT d_I=385μm, X=0.43, T23.

The analysis of the experimental data shown in Figures 10, 11 and 12 suggests that for larger particles, that in present work are those with a diameter equal to 1.59 and 3 mm, the main resistance is due to the dissolution (Figure 11). Instead, for the smallest particles, that have a diameter equal to 0.375 mm, the dissolution resistance is negligible with respect to that due to the mixing/diffusion. In particular, for the working conditions analyzed in this work, for the smallest particle size the diffusion in the stagnant free liquid layer is the slowest step (Figure 10).

5. Conclusions

Dissolution and mixing in dilute and dense solid-liquid systems have been analysed by experimental data obtained with ERT, in two standard-geometry stirred tanks of different size equipped with different impellers. The experiments were carried out to compare the behaviour of dilute and dense mixtures with the goal of identifying the effect of the presence of a clear liquid layer in the tank, of the size of the soluble particles and of the agitation conditions.

Since both the mixing and the dissolution processes can be characterized measuring the conductivity change due to the dissolution and the dispersion of a conductive species, the ERT technique is particularly suitable for following the dynamics of the two process.

The analysis of the experimental data suggests that three different resistances can influence the dynamic evolution of the local conductivities before achieving homogeneity. Depending on the working conditions in the stirred tank, the particle dissolution, the convective mixing or the diffusion in the stagnant liquid layer can assume the prevalent role.

Starting from literature correlations and based on a new correlation, that is necessary to extend the applicability of the Bittorf and Kresta correlation for the cloud height estimation, a new approach is suggested to identify the main mass transfer resistance taking place when the mixing or the dissolution of a soluble solid has to be accomplished in dense or dilute solid-suspensions.

The new approach can be used for analysing the effect of tank/impeller geometry, impeller speed, solid concentration and particle size with the goal of identifying the working conditions that intensify solid-liquid mass transfer in mechanically stirred tanks. The adoption of additional impellers as an alternative to the single impeller configuration considered in this work can also be taken into account for energetic optimization.

Finally, to predict the main mass transfer resistance for homogenization and dissolution processes a diagram as that reported in Figure 2 can be used. The parameter on the left side of the triangle will be t_d/t_m, the parameter on the right side will be t_{diff}/t_m and the parameter on the bottom side will be t_d/t_{diff}. Depending on the position of the point determined by the values of the three parameters, the main resistance of the process will be identified.

Notation

Ar = Achimedes number $\frac{g d_p^3 \rho_l (\rho_s - \rho_l)}{\mu^2}$ (-)

C = clearance (m)

C_i =dimensionless conductivity in the cell i (-)

C_{bulk} = salt concentration in the bulk fluid (g/L)

C_{sat} = salt concentration at saturated conditions (g/L)

D = impeller diameter (m)

D_j= diffusion coefficient of species j (m^2/s)

d_p= soluble mean particle diameter (m)

d_I= inert mean particle diameter (m)

g = gravity acceleration (m/s^2)

H_L = liquid height (m)

H_C = cloud height (m)

k_L = mass transfer coefficient (m/s)

k_{diff} = mass transfer coefficient by diffusion (m/s)

N = impeller speed (1/s)

N_{js} = just suspended impeller speed (1/s)

N_{min} = minimum impeller speed for suspension, Eq. 15 (1/s)

N_{span} = characterisitc impeller speed, Eq. 15 (1/s)

N_Q = impeller flow number (-)

Re_p = particle Reynolds number $\frac{\pi N D d_p \rho_l}{\mu}$ (-)

Sc = Schmidt number $\frac{\mu}{\rho_l D_j}$ (-)

Sh = Sherwood number$\frac{k_L d_p}{D_j}$ (-)

t = time (s)

t_d = dissolution time (s)

t_{diff} = diffusion characteristic time (s)

t_m = mixing time (s)

t_r = contact time (s)

T = tank diameter (m)

x = level of homogeneity, Eq 5 (%)

X= mass ratio of inert solid to liquid (-)

X_S= fraction of the suspended solid, Eq. 15 (-)

X_{US}= mass fraction of the unsuspended solid (-)

z_i= axial coordinate of the measurement planes (m)

Subscripts and apexes

95 = 95% of liquid homogeneity (-)

99.9 = 99.9% of liquid homogeneity (-)

Greek symbols

χ = normalized dimensionless conductivity (-)

μ = liquid dynamic viscosity (Pa s)

ρ_i = inert particle density (kg/m^3)

ρ_l = liquid density (kg/m^3)

ρ_s = dissolving particle density (kg/m^3)

$\tau_{dis,dil}$ = experimental dissolution time in dilute systems (s)

$\tau_{mix,dense}$ = experimental mixing time in dense systems (s)

$\tau_{dis,dense}$ = experimental dissolution time in dense systems (s)

References

Atiemo-Obeng, V.A., Penney, W.R., Armenante, P., Solid-liquid Mixing, Chapter 10, p. 545 in Paul, E. L.; Atiemo-Obeng, V. A.; Kresta, S. M. Handbook of Industrial Mixing: Science and Practice; John Wiley & Sons, Hoboken, NJ, 2004.

Bittorf, K.J., Kresta, S.M., 2003. Prediction of cloud height for solid suspensions in stirred tanks. Chem. Eng. Res. Des. 81(5), 568-577. https://doi.org/10.1205/026387603765444519.

Bong, E.Y., Eshtiaghi, N., Wu, J., Parthasarathy, R., 2015. Optimum solids concentration for solids suspension and solid-liquid mass transfer in agitated vessels (2015). Chemical Engineering Research and Design, 100, 148-156. https://doi.org/10.1016/j.cherd.2015.05.021.

Brunazzi, E., Galletti, C., Paglianti, A., Pintus, S., 2004. An impedance probe for the measurements of flow characteristics and mixing properties in stirred slurry. Chem. Eng. Res. Des. 82(9 SPEC. ISS.), 1250-1257. https://doi.org/10.1205/cerd.82.9.1250.44165.

Bujalski, W., Takenaka, K., Paolini, S., Jahoda M., Paglianti A., Takahashi K., Nienow, A.W., Etchells, A.W., 1999. Suspension and liquid homogenization in high solids concentration stirred chemical reactors. Chem. Eng. Res. Des. 77(3), 241-247. https://doi.org/10.1205/026387699526151.

Carletti, C., Bikic, S., Montante, G., Paglianti, A., 2018. Mass transfer in dilute solid−liquid stirred tanks. Ind. Eng. Chem. Res. 57(18), 6505-6515. https://doi.org/10.1021/acs.iecr.7b04730.

Carletti, C., Blasio, C. D., Mäkilä, E., Salonen, J., Westerlund, T., 2015. Optimization of a Wet Flue Gas Desulfurization Scrubber through Mathematical Modeling of Limestone Dissolution Experiments. Ind. Eng. Chem. Res., 54 (40), 9783-9797. https://doi.org/10.1021/acs.iecr.5b02691

Carletti, C., Montante, G., De Blasio, C., Paglianti, A., 2016. Liquid mixing dynamics in slurry stirred tanks based on electrical resistance tomography. Chem. Eng. Sci. 152, 478-487. https://doi.org/10.1016/j.ces.2016.06.044.

El-Naggar, M. A., Abdel-Aziz, M. H., Zatout, A. A., Sedahmed, G. H., 2014. Liquid-Solid Mass Transfer Behavior of a Stirred-Tank Reactor with a Fixed Bed at Its Bottom. Chem. Eng. Technol. 37 (9), 1525-1531. https://doi.org/10.1002/ceat.201300689|.

Grenville, R.K., Nienow, A.W., Blending of miscible liquids, Chapter 9 in Paul, E. L.; Atiemo-Obeng, V. A.; Kresta, S. M. Handbook of Industrial Mixing: Science and Practice; John Wiley & Sons, Hoboken, NJ 2004.

Hofinger, J., Sharpe, R.W., Bujalski, W., Bakalis, S., Assirelli, M., Eaglesham, A., Nienow, A.W., 2011. Micromixing in two-phase (G-L and S-L) systems in a stirred vessel. Can. J. Chem. Eng., 89 (5), 1029-1039. https://doi-org.ezproxy.unibo.it/10.1002/cjce.20494.

Hörmann, T., Suzzi, D., Khinast, J. G., 2011. Mixing and Dissolution Processes of Pharmaceutical Bulk Materials in Stirred Tanks: Experimental and Numerical Investigations. Ind. Eng. Chem. Res., 50 (21), 12011-12025. https://doi.org/10.1021/ie2002523.

Kikuchi, K.-I., Tadakuma, Y., Sugawara, T., Ohash, H., 1987. Effect of inert particle concentration on mass transfer between particles and liquid in solid-liquid two-phase upflow through vertical tubes and in stirred tanks. Journal of Chemical Engineering of Japan, 20 (2), 134-140. DOI: 10.1252/jcej.20.134.

Kraume, M., 1992. Mixing times in stirred suspensions. Chem. Eng. Technol., 15 (5), 313-318. https://doi.org/10.1002/ceat.270150505|

Lee, T., Hou, H. J., Hsieh, H. Y., Su, Y. C., Wang, Y. W., Hsu, F. B., 2008. The Prediction of the Dissolution Rate Constant by Mixing Rules: The Study of Acetaminophen Batches. Drug Dev. Ind. Pharm. 34 (5), 522-535. https://doi.org/10.1080/03639040701744194

Magelli, F., Montante, G., Pinelli, D., Paglianti, A., 2013. Mixing time in high aspect ratio vessels stirred with multiple impellers. Chem. Eng. Sci. 101, 712-720. https://doi.org/10.1016/j.ces.2013.07.022

Micale, G., Grisafi, F., Brucato, A., 2002. Assessment of particle suspension conditions in stirred vessels by means of pressure gauge technique. Chem. Eng. Res. Des. 80(8), 893-902. https://doi.org/10.1205/026387602321143444.

Mishra, P., Ein-Mozaffari, F., 2020. Critical review of different aspects of liquid-solid mixing operations. Rev. Chem. Eng., 36 (5), 555-592. https://doi.org/10.1515/revce.

Montante, G., Paglianti, A., 2015. Gas hold-up distribution and mixing time in gas-liquid stirred tanks. Chem. Eng. J. 279, 648-658. https://doi.org/10.1016/j.cej.2015.05.058.

Nienow, A. W., Miles, D., 1978. The effect of impeller/tank, configurations on fluid-particle mass transfer . Chem. Eng. J. 15 (1), 13– 24. DOI: https://doi.org/10.1016/0300-9467(78)80033-1.

Paglianti, A., Carletti, C., Montante, G., 2017. Liquid Mixing Time in Dense Solid-Liquid Stirred Tanks. Chem. Eng. Technol. 40(5), 862-869. https://doi.org/10.1002/ceat.201600595.

Paglianti, A., Maluta, F., Montante, G., 2020. Particles dissolution and liquid mixing dynamics by Electrical Resistance Tomography. T. I. Meas. Control. 42(4), 647-654. https://doi.org/10.1177/0142331219842318

Sardeshpande, M.V., Sagi, A.R., Juvekar, V.A., Ranade, V.V., 2009. Solid suspension and liquid phase mixing in solid-liquid stirred tanks. Ind. Eng. Chem. Res. 48(21), 9713-9722. https://doi.org/10.1021/ie801858a

Stanley, S.J., Mann, R., Primrose, K., 2002. Tomographic imaging of fluid mixing in three dimensions for single-feed semi-batch operation of a stirred vessel. Chem. Eng. Res. Des. 80(8), 903–909. https://doi.org/10.1205/026387602321143453.

Stoian, D., Eshtiaghi, N., Wu, J., Parthasarathy, R., 2017. Enhancing Impeller Power Efficiency and Solid-Liquid Mass Transfer in an Agitated Vessel with Dual Impellers through Process IntensificationIndustrial and Engineering Chemistry Research, 56 (24), 7021-7036. https://doi.org/10.1021/acs.iecr.7b00435.

Tokura, Y., Uddin, M.A., Kato, Y., 2019. Effect of Suspension Pattern of Sedimentary Particles on Solid/Liquid Mass Transfer in a Mechanically Stirred Vessel, Industrial and Engineering Chemistry Research, 58 (24), 10172-10178. https://doi.org/10.1021/acs.iecr.9b00594.

Treybal, R.E. Mass-Transfer Operation, third edition; McGraw-Hill, Singapore. 1981.

Tschentscher, R., Spijkers, R. J. P., Nijhuis, T. A., Van Der Schaaf, J., Schouten, J. C., 2010. Liquid- Solid Mass Transfer in Agitated Slurry Reactors and Rotating Solid Foam Reactors. Ind. Eng. Chem. Res., 49 (21), 10758-10766. https://doi.org/10.1021/ie100385n

Williams, R.A., Beck, M.S. Process Tomography: Principles, Techniques and Applications; Butterwirth-Heinemann, Oxford. 1995.